Decoding auditory working memory content from intracranial high frequency activity in humans

Işıl Uluç * [1,2,3], Noam Peled [1,2,3], Angelique C. Paulk [2,3], Alan Bush [2,3], Valentina Gumenyuk [4], Parker Kotlarz [1], Kaisu Lankinen [1,2,3], Fahimeh Mamashli [1,2,3], Nao Matsuda [1,2], Mark R. Richardson [2,3], Steven M. Stufflebeam [1,2,3], Sydney S. Cash [2,3] & Jyrki Ahveninen [1,2,3]

[1] Athinoula A. Martinos Center for Biomedical Imaging, Department of Radiology, Massachusetts General Hospital, Charlestown, MA, USA
[2] Massachusetts General Hospital, Boston, MA, USA
[2] Department of Radiology, Harvard Medical School, Boston, MA, USA
[4] University of Nebraska Medical Center

Corresponding author *:
Işıl Uluç, Ph.D.
CNY 149, 13th St.
A.A. Martinos Center for Biomedical Imaging,
Department of Radiology,
Massachusetts General Hospital,
Charlestown, MA 02129
iuluc@mgh.harvard.edu
Tel: 617 726 6584, Fax: (617) 726-7422

Abstract

How the human brain maintains information in working memory (WM), a process critical for all our goal-directed function, has been debated for decades. Classic neurophysiological models, which argue that WM is maintained via persistent content-specific "delay activity", have been challenged by alternative ideas suggesting a combination of dynamic activity patterns and activity-silent mechanisms. Here, making use of human intracranial stereo-EEG (sEEG) recordings and machine learning techniques, we tested understudied auditory WM in multiple cortical and subcortical brain areas. Neuronal activity was quantified as broadband high frequency activity (HFA, 70-190 Hz), which has been shown to be highly correlated with multiunit activity of neuron populations. Our multivariate pattern analysis (MVPA) results, validated via robust non-parametric permutation testing, show that information can be decoded from multiple brain areas including frontal and auditory areas as well as hippocampus. However, the recording sites with high decoding accuracies were not accompanied by statistically significant increases in HFA power. In contrast, HFA power was reduced relative to the pre-trial period in many in frontal, auditory cortex, and hippocampal sEEG recording sites. These results are in line with the hypothesis that WM maintenance can be supported by highly dynamic activity silent processes, rather than via persistent activity only.

Introduction

Working memory (WM) is crucial for goal-directed cognitive functions that enable us to maneuver the world. One of its behaviorally most relevant, and theoretically least understood, domains is auditory WM, a process essential for our ability to communicate, socialize, and operate with purpose in our dynamic everyday environments.

The neuronal mechanisms of WM have been a focus of intensive neuroscience research since 1970's (Baddeley and Hitch, 1974; D'Esposito and Postle, 2015). Investigating how and where the WM information is maintained, non-human primate (NHP) and non-invasive human imaging studies gave valuable insight into the mechanisms underlying WM processing. The emphasis of this discussion has, increasingly, been shifting from the "where in the brain is WM maintained" the neurophysiological nature of these maintenance processes. Different theories were proposed to explain how neuronal processes that enable WM maintenance work (Barak and Tsodyks, 2014; Stokes, 2015; Christophel et al., 2017; Miller et al., 2018).

The debate of what the nature of neuronal processes underlying WM maintenance started with the initial WM studies in non-human primates (NHP), showing consistent firing in PFC (Fuster and Alexander, 1971; Rosenkilde et al., 1981). The neurophysiological studies suggested that a sustained delay activity maintains the information throughout WM retention (Goldman-Rakic, 1995; Romo et al., 1999; Constantinidis and Procyk, 2004; Vergara et al., 2016). Subsequent human neuroimaging studies (Christophel et al., 2012; Christophel and Haynes, 2014; D'Esposito and Postle, 2015), however, show that content-specific information could also be found in posterior brain areas where no sustained activity is present during WM maintenance. Evidence is also emerging that not only are posterior and sensory areas involved in WM maintenance, but the neuronal processes maintaining WM do not necessarily depend on persistently elevated neuronal firing. The smaller number of neurophysiological studies in the auditory domain are consistent with this notion, suggesting that persistent delay-period spiking patterns, which were reported in certain early NHP and rodent studies(Gottlieb et al., 1989; Sakurai, 1990), do not necessarily carry information about the maintained content(Bigelow and Poremba, 2014; Ng et al., 2014; Scott et al., 2014).

The dichotomy between neurophysiological recordings in NHPs and human non-invasive studies has elicited different theories on the nature of the WM process and the reinterpretation of old findings regarding the persistent neuronal firing during the delay period. A number of more recent neurophysiological studies support an interpretation that persistent firing during the WM delay period is a correlate of other brain functions including attention decision-making, learning, or motor preparation (Lundqvist et al., 2018a; Sreenivasan and D'Esposito, 2019). At the same time, while the classic studies were based on trial-averaged signals, more recent studies using single-trial analysis approaches (Shafi et al., 2007; Lundqvist et al., 2016) suggest more dynamic mechanisms that involve a combination of sparce bursting rather than persistent spike activity and synaptic-plasticity mechanisms (Lundqvist et al., 2016; Kucewicz et al., 2017; Bastos et al., 2018; Lundqvist et al., 2018b). However, these alternative theories are criticized to be inconsistent with the neurophysiological findings regarding the neuronal underpinnings of WM. Persistent activity, albeit not a time varying one, is found to be correlated with the memoranda and the criticism is lacking considering these findings. Moreover, alternative models of WM have been mostly inspired by functional imaging studies, and although they in theory attractive, they are very limited due to their nature and fail to account for WM behavior (Constantinidis et al., 2018).

The insight about WM-related local neuronal circuits mostly come from NHP studies, primarily conducted in visual and tactile domains (Goldman-Rakic, 1995; Romo et al., 1999; Barak et al., 2010). However, the simple delayed-match-to-sample designs in highly trained laboratory animals have not been optimal for differentiating between cognitive functions such as adaptive learning, long-term, and working memory. This difficulty is, perhaps, most evident in the domain of auditory WM, as complex auditory-cognitive tasks are very difficult to learn for NHPs(Fritz et al., 2005; Scott et al., 2012; Scott and Mishkin, 2016). In the auditory domain of WM, this limitation leaves us mostly dependent on human neuroimaging studies(Lutzenberger et al., 2002; Kaiser et al., 2007; Kaiser, 2015; Kumar et al., 2016; Uluç et al., 2018; Ahveninen et al., 2023). An inherent difficulty of resolving this debate has been the difficulty of obtaining high resolution neurophysiological recordings in humans. One potential way to bridge the gap between animal

models and human neuroimaging studies is to use intracranial EEG recordings in presurgical human patients.

Utilizing their high signal-to-noise ratio (SNR), human intracranial studies inquire into the higher end of the oscillatory signals and broadband high frequency (HFA) of neuronal activity to further investigate neural correlates of WM. Gamma power (30-60Hz) has been shown to be modulated as a function of memory content during WM retention (Howard et al., 2003; Kaiser et al., 2008), and high gamma is tightly correlated with successful WM performance (Yamamoto et al., 2014) (65-120Hz). Additionally, the HFA (70-200Hz) is argued to reflect local neuronal spiking (Ray et al., 2008; Leszczynski et al., 2020). Ray and colleagues (2008) showed that HFA in the LFP was strongly temporarily correlated with the average firing rate recorded by the microelectrodes on a trial-by-trial basis as opposed to low gamma (40-80 Hz). These findings suggest that multiunit activity (MUA) is a direct correlate of HFA (although see also Leszczynski et al. 2020). This direct correlate of MUA is shown to play a role in WM maintenance. However, it is still ambiguous if the HFA is a direct correlate of WM maintenance or executive processes aiding WM, such as attention.

To this aim, we designed a retro-cue task to record neurophysiological signals from sEEG electrodes during auditory WM maintenance. Auditory tasks were utilized, not only because the disproportionately small number of previous neurophysiological studies relative to visual and tactile domains, but also because the (solely) clinically dictated implantation plans encompassed much of the cortical auditory processing hierarchy in our participants. In our task, we used auditory nonconceptual complex modulation patterns (ripple sounds) to ensure that the information maintained is nonverbal but processed speechlike (for a more detailed explanation, see Mamashli et al., 2021). We then decoded activity patterns from LFP HFA patterns. To investigate the time course of the whole signal in more detail, we also decoded the information from intracranial event-related potentials (iERP) elicited during the maintenance period. Our results propose that WM content information is stored in HFA patterns from the bilateral superior temporal cortex (STC), hippocampus (HC), and inferior frontal gyrus (IFG). Depending on these results, we suggest that HFA is a neural correlate of WM maintenance.

Methods

Participants

We collected stereo-EEG (sEEG) data from thirteen participants (n=13, Female = 6, Male = 7 ; age=33.39±10.9 - ages are jittered for deidentification purposes) who were implanted mainly in frontal and temporal brain regions. The subjects had varying types of epilepsy with pharmaco-resistant complex partial seizures. Data of one participant was excluded due to insufficient number of trials. The data was collected while subjects were undergoing invasive monitoring for surgical evaluation. The electrode implantations were made exclusively on clinical grounds as a part of diagnostic procedure. All participants provided written fully informed consent. The study design, protocol, and consent form were approved by the Mass General Brigham Institutional Review Board.

Stimuli and Procedure

Participants performed a retro-cue WM task with simultaneous recordings of behavior and sEEG from both cortical and subcortical brain structures. In our auditory WM experiment, we employed broadband sound patterns modulated across time (ripple velocity, ω cycles/s) and frequency (Ω cycles/octave), ripple sounds as memory items. Ripple sounds were chosen as memoranda as they have speech-like patterns spectrotemporally (Shamma, 2001) but are not contaminated by conceptual properties (Fig. 1a). There were four 750-ms ripple sounds with different ripple velocities that were modified based our previous studies (Mamashli et al., 2021; Ahveninen et al., 2023). To make the task feasible for our subjects during their clinical visit, we determined the ripple velocities based on the largest just-noticeable-difference observed among the participants in our previous study. The ripple velocities for the four item classes were 9.5, 18.2, 34.9, and 66.8 cycles/s. Two additional velocities were used for probes, including 5.0 and 128 cycles/s. Sound stimuli were delivered by loudspeakers (JBL Wireless Go 2, Harman I.I.Inc,

USA / Cyber Acoustics Sound Bar USB Speaker, Cyber Acoustics inc. ,USA) externally connected to the presentation computer.

The retro-cue WM paradigm, which is well established in the field (Christophel et al., 2012; Christophel and Haynes, 2014; Uluç et al., 2018; Ahveninen et al., 2023), aims to dissociate perception and attention from memory maintenance (Fig. 1). It is essentially a modification of a delayed match to sample paradigm. In our WM task, we sequentially presented two 750-ms ripple sounds with a 250-ms interstimulus interval (ISI). The second ripple sound was followed by a retro-cue indicating the item to remember. The visual retro-cue consisted of a visual "memorize1" or "memorize2" cue- after another 250-ms ISI. After a 3-s maintenance period, in the middle of which an unrelated sound stimulus (50ms white noise) is presented, a ripple sound probe is presented with a same/different response scheme. Participant gave a self-paced response by pressing A (same) and S (different) button presses on the keyboard indicating if the test probe is the same as the memorized item or not. After each trial a 1-s inter trial interval was registered (Fig. 1).

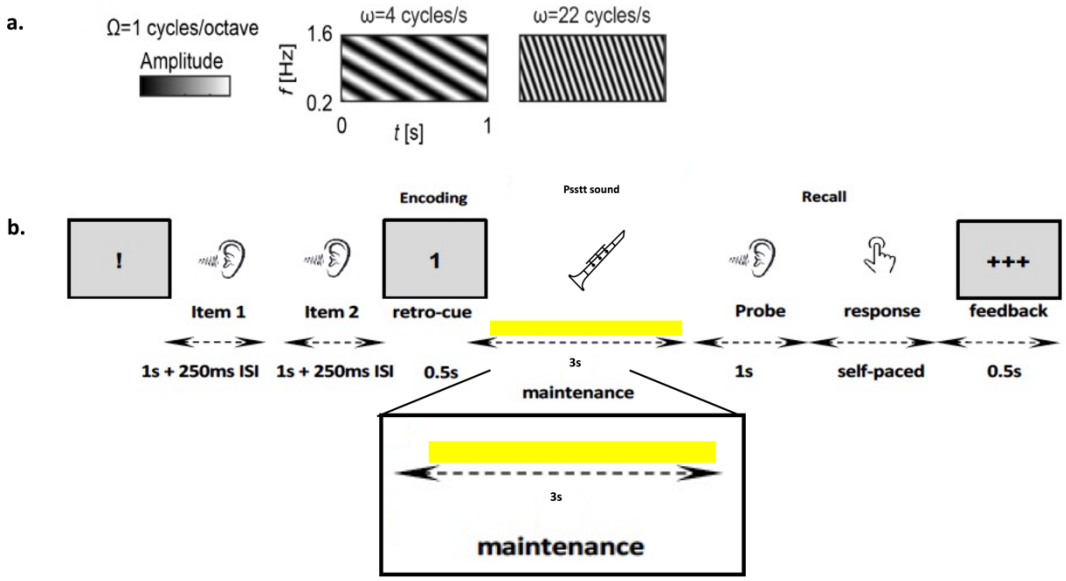

Figure 1. Diagram of the stimuli and paradigm. **(a)** visualization of the spectratemporal pattern of ripple sound stimuli. **(b)** Timecourse of the WM task. Presentation of ripple sounds were denoted by waves to the ears and the

impuse sound was denoted by an instrument. Participants were instructed to press button in a self-paced manner and provided with feedback after response.

In each run there were 24 trials in total. 12 of the trials were match and the other 12 trials were non-matching trials. The non-match trials were divided into two with half the trials complete non-match trials where the probe was a different ripple sound from the two items that are presented at the beginning of the trial. The other half of the non-matching trials was so that the probe was the uncued item. The memory items were pseudo-randomly chosen from four different classes with different temporal frequencies. To eliminate categorical encoding, participants were left naïve to the number of items to memorize. The task was planned to be 120 trials in total if completed with 5 runs. The number of trials completed changed among participants as they were admitted to epilepsy monitoring unit as a part of their clinical diagnosis procedure at the time.

Data Acquisition

sEEG was recorded from a montage of 8-18 unilaterally or bilaterally implanted depth electrodes depending on the clinical diagnosis procedure of the participant. Intracranial signals were recorded using a recording system with a sampling rate of 2 kHz (Neural Signal Processor, Blackrock Microsystems, US) or with a sampling rate of 1kHz (European Data Format, EDF). At the time of acquisition, sEEG recordings were referenced to an EEG electrode that was placed on the head (either cervical vertebrae 2 or Cz or a sEEG contact that, based on imaging localization, in the skull and outside the brain.).

Electrodes were localized by an established a volumetric image co-registration procedure that is used for clinical application. First, the pre operation T1-weighted MRI images were aligned post operation CT or MRI images that show electrode locations using Freesurfer scripts (http://surfer.mnr.mgh.harvard.edu). Electrode coordinates were manually determined from the post operation images. The electrodes were then mapped to standard cortical parcels/regions using the MMVT toolbox (Felsenstein et al., 2019; Soper et al., 2023).

The MMVT toolbox uses an automatic, probabilistic labeling algorithm that calculates the distances from and probability of each contact for each cortical and subcortical label using Electrodes Labeling Algorithm (ELA, https://github.com/pelednoam/ieil ; Peled et al., 2017). ELA identifies the nearest brain region label by creating an expanding cylinder around each electrode and calculating the probability of overlap of this cylinder with identified cortical and subcortical structure labels(Soper et al., 2023). We used the Lausanne500 parcellation atlas (Daducci et al., 2012) in addition to a subcortical mapping (Fischl et al., 2004; Desikan et al., 2006; Reuter et al., 2010; Reuter et al., 2012) for mapping the electrodes' locations The electrodes that were within or less than 1.5mm distance from cortical areas were taken as cortical electrodes. The electrodes within 2.5mm distance from the centroid of the subcortical region are taken as subcortical electrodes. As our regions of interest, we chose auditory cortex (AC), the inferior frontal gyrus (IFG), and the hippocampus (HC), which have been previously related to WM maintenance. We also included the orbitofrontal gyrus (OFG) contacts, because of its strong anatomical connection to the monkey AC (Medalla and Barbas, 2014) and possible association with human auditory WM (Mamashli et al., 2021).

For the visualization of results in a common anatomical template, all contacts from all subjects are resampled to Colin27-space using MMVT and ELA algorithm. Lausanne500 parcellation atlas and subcortical mapping was performed in the common space in the same manner as in native space.

Preprocessing

Data was preprocessed with custom MATLAB scripts using Fieldtrip toolbox (Oostenveld et al., 2011). The data was divided into single-trial epochs starting from 300 ms before to 3 s after the retro-cue onset. Bad channels and epochs are found and rejected based on visual evaluation. The data were detrended with a baseline window of -300ms to 0ms, and filtered with a 300Hz low pass and a 0.1Hz high pass filter sequentially using *ft_preprocessing*. Notch filtering was used to remove 60 Hz line noise from the data. Blackrock datasets were downsampled to 1 kHz. Whole

trial datasets were detrended and both EDF and Blackrock datasets were downsampled to 1 kHz. Data were then re-referenced to average of all electrodes remaining electrodes. After the spectral analysis, the outlier trials for each contact are calculated using MATLAB's built-in outlier function and contacts with more than 5 outlier trials were rejected from further analysis.

Main analyses

Spectral Analysis

Epochs between -0.3 and 3 s with the onset at retro-cue were used for the time frequency analysis for each contact for each trial. Time frequency representations (TFR) of spectral power between 70Hz and 190Hz were computed with a Morlet wavelet transformation of seven cycles length sliding window at 2 Hz intervals in the time domain, baseline corrected relative to the 300-ms pre-cue period and averaged across the frequency bins to yield the HFA time course for estimating content-specific patterns of brain activity during WM maintenance.

To examine the full trial HFA patterns, we calculated HFA time courses also across the entire 9-s trial period in the same fashion. The power is corrected to absolute baseline of 300 ms before the onset of the first sound item and averaged across frequency bins. HFA changes related to WM maintenance were estimated in each participant, contact, and time point using one-sample t-tests across individual trials. To make sure we do not miss any HFA increases that emerge during maintenance, the results are reported without conservative post hoc corrections. That is, the purpose was to avoid the Type II error, rejecting the persistent activity model due to using conservative thresholding. The results of these analyses are plotted as -log10(p) values, multiplied with the sign of the t in each time point, thresholded at $p<0.05$.

HFA Decoding Analysis

We employed a four-class classification with a support vector machine (SVM) classifier to decode the memorized items from sEEG HFA power during the WM maintenance. For SVM, we utilized SVM implemented in libsvm (Chang and Lin, 2011) and provided in the COSMOMVPA package (Oosterhof et al., 2016) in MATLAB. SVM decoding accuracies were calculated based on median HFA power in sliding 500 ms windows (200 steps in the 3.3 s period, i.e., 16.5 ms steps) for each contact. To enhance the SNR, subaverages of four trials were calculated with each class using *cosmo_average_samples*. 50 different random iterations were calculated of these subaveraged samples. Four-fold cross-validation was utilized for each iteration: the model was trained in 75% of the samples and tested in the remaining samples. *cosmo_nfold_partitioner* was used to ensure that the number of trials were balanced for each condition and the training and test data were separate. The decoding accuracies were averaged across the folds and iterations.

In the common space, a weighted decoding value is determined for each cortical label by the weighted average of subjects with significant decoding accuracy for this cortical label. In the case where a subject had more than one contact with a significant decoding accuracy for this cortical label, we selected the contact with the highest decoding accuracy. We repeated this procedure for each time point in the maintenance period decoding analysis. For visual feasibility, 180 timepoint map figures were downsampled to 9 decoding accuracy maps throughout the maintenance period using sliding windows. The common space decoding accuracy maps were generated using MMVT.

Time-Domain iERP Decoding Analysis

As in HFA decoding, we employed a four-class SVM classification on the preprocessed signals from the sEEG electrodes. We calculated the SVM decoding accuracy using the temporal information within the 500-ms sliding time window at 20-ms steps. To enhance SNR, individual

trials were pooled to subaverages of 4 trials within each class using *cosmo_average_samples*. The same analysis was repeated across 50 random iterations of these subaveraged samples. Four-fold cross-validation was utilized for each iteration so that the model was trained in 75% of the samples and tested in the remaining 25% of the samples. The decoding accuracies were averaged across the folds and iterations.

Statistical Significance

Robust maximum-statistic permutation test strategy is utilized for dealing with multiple comparisons in the testing of decoding hypotheses. For both HFA and ERP decoding analyses, the statistical significance was calculated using a cluster-based maximum statistic permutation test with 500 permutations. The uncorrected cluster-forming threshold was determined non-parametrically, defined as the percentile 99 of full distribution of decoding accuracies across all permutations in all contacts. We calculated the thresholds for each hemisphere separately because most subjects were implanted unilaterally. Finally, the clusters of decoding accuracy over the threshold and a cluster-wise corrected p value were calculated for each electrode (containing 8-16 contacts).

Control Analyses

HFA Decoding Analysis on Uncued items

To control whether the SVM classification indicated memory information, we performed MVPA on HFA power for trials according to uncued items. The parameters for spectral analysis and SVM 4-class classification were the same as cued item analyses. The only difference was that the trials were defined according to the uncued item code.

Results

We studied human auditory WM using a ripple-sound retro-cue task in 12 participants under intracranial monitoring. Our multivariate pattern analyses suggest that maintained auditory WM content can be decoded from dynamic patterns of brain activation patterns, in the absence of persistently elevated activity relative to pre-trial baseline. WM content could be decoded from dynamic changes in broadband HFA, a putative correlate of concurrent firing activity, as well as from temporal patterns of intracranial event-related potentials (iERP).

Behavioral Performance

Participants (n=12) performed with 62.95±3.44 (mean±SEM) with correct responses across all trials of a retro-cue paradigm. We performed an ANOVA with four levels to test if recall performance changes in relation to memorized ripple velocity. Our analysis showed no significant difference between the behavioral performance per memorized ripple velocity.

Multivariate Analysis of Broadband HFA during WM Maintenance

Evidence for significant WM decoding results ($p<0.05$, maximum-statistic permutation test) using HFA data was found in all participants. **Figures 2-7** show the results of four-class SVM classification in four brain areas that have previously been reported to maintain WM information in auditory (Uluç et al., 2018; Mamashli et al., 2021; Ahveninen et al., 2023) or other domains (Schmidt et al., 2015; Wu et al., 2018), including auditory cortex (AC), the inferior frontal gyrus (IFG), and the hippocampus (HC). In addition, we also analyzed contacts within the orbitofrontal gyrus (OFG), given its strong domain-specific anatomical connectivity to the monkey AC (Medalla and Barbas, 2014) and possible association with human auditory WM (Mamashli et al., 2021). SVM classification was applied to the medial power of HFA with a 500ms sliding window from the

3.3-s maintenance period. In all analyses, the statistical significance was calculated using a cluster-based maximum-statistic permutation test with 500 permutations.

Our AC analysis area includes contacts in Heschl's gyri (HG) and superior temporal gyri (STG) in the hemispheres the subjects were implanted with. In total, nine out of the 12 subjects had contacts in these areas. The significance for the decoding accuracies was calculated for each hemisphere separately because several of our subjects had sEEG contacts implanted in only in one hemisphere. Our HFA decoding results in AC sEEG contacts show continuous clusters of significant decoding accuracy on six of these subjects. In four these subjects, statistically significant above chance decoding accuracies spread throughout the whole maintenance period (Fig. 2d).

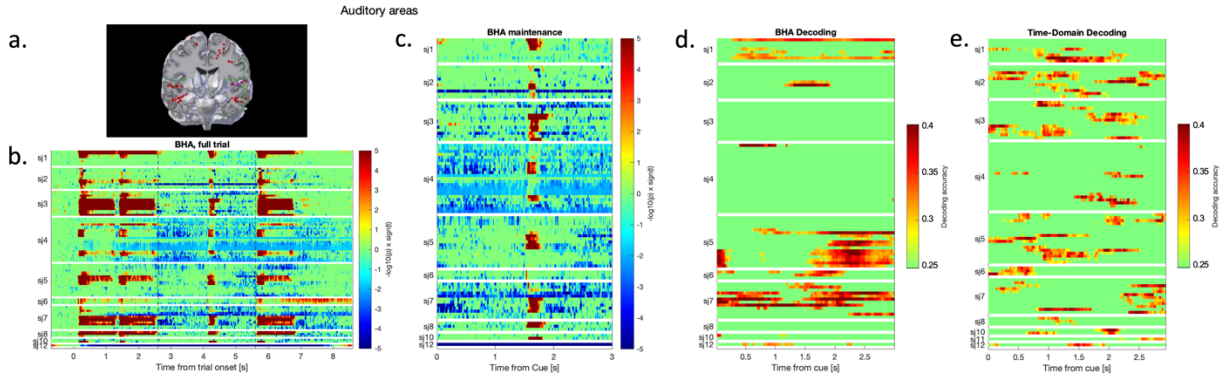

Figure 2. Auditory contacts and time courses. (**a)** example of electrodes that were implanted in AC. All results here are demonstrated for IFG contacts within or less than 1.5mm to the cortical label. **(b)** Whole trial HFA power time course. **(c)** Working memory period for HFA time courses. **(d)** HFA decoding analyses for IFG contacts for all subjects (e) Time-domain decoding analysis from the iERP data. The decoding results have been thresholded based on a cluster-based maximum-statistic permutation test in each subject ($p<0.05$).

In total, 11 out of our 12 subjects had contacts that were recording from IFG. From these 11 subjects, we found continuous clusters of decoding accuracies that were significantly above chance level in eight subjects. However, for most of these contacts, the significant clusters were limited to either in the first half or the second half of the maintenance period only (Fig. 3d).

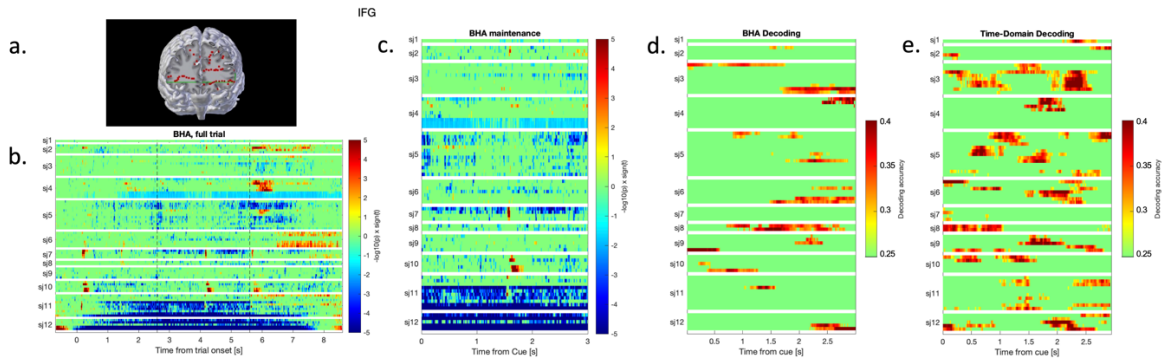

Figure 3. IFG contacts and time courses. (**a)** example of electrodes that were implanted in IFG. All results here are demonstrated for IFG contacts within or less than 1.5mm to the cortical label. **(b)** Whole trial HFA power time course. **(c)** Working memory period for HFA time course. **(d)** HFA decoding analyses for IFG contacts for all subjects. **(e)** Time-domain decoding analysis from the iERP data. The decoding results have been thresholded based on a maximum-statistic permutation test in each subject (p<0.05).

Data from OFG contacts were available in ten of our 12 subjects. Although the number of recording contacts showing significant decoding accuracy within each subject was smaller for this region, six out of ten subjects had contacts that had continuous decoding clusters. Furthermore, two of those subjects had decoding accuracies spread throughout the whole maintenance period in OFG contacts (Fig. 4d).

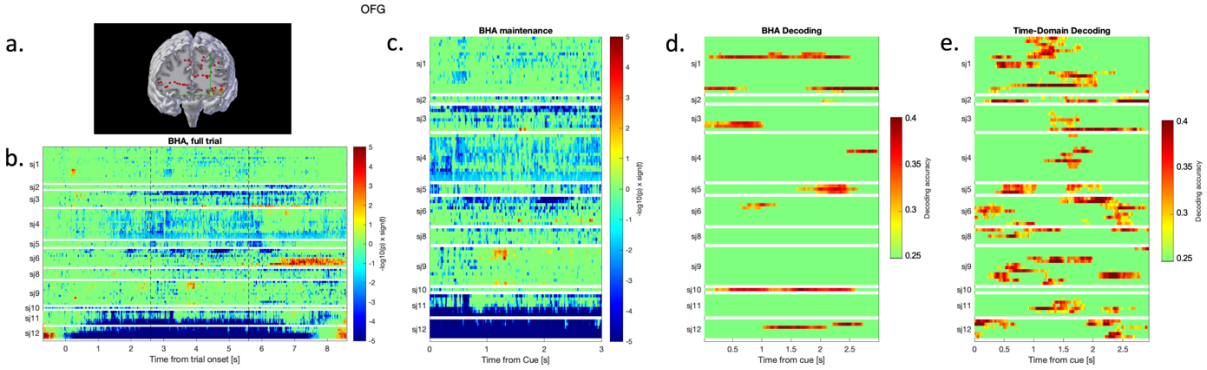

Figure 4. OFG contacts and time courses. (**a)** example of electrodes that were implanted in OFG. All results here are demonstrated for IFG contacts within or less than 1.5mm to the cortical label. **(b)** Whole trial HFA power time course. **(c)** Working memory period for HFA time course **(d)** HFA decoding analyses for IFG contacts for all subjects **(e)** Time-

domain decoding analysis from the iERP data. The decoding results have been thresholded based on a cluster-based maximum-statistic permutation test in each subject (p<0.05).

Data from contacts within HC was available from ten out of the 12 subjects. Out of these ten subjects, we observed significant decoding in six subjects, with 4 of these subjects showing significant decoding results during the entire maintenance period (Fig. 5d).

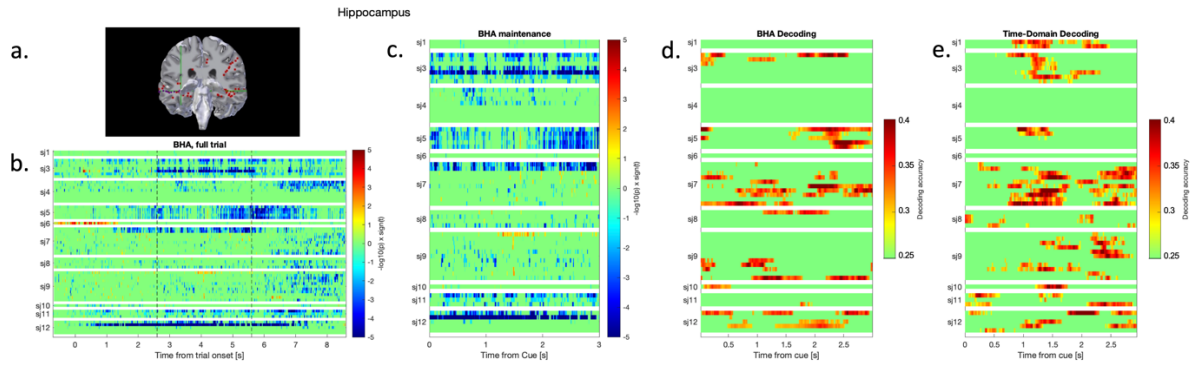

Figure 5. HC contacts and time courses. (**a)** example of electrodes that were implanted in HC. All results here are demonstrated for IFG contacts within or less than 1.5mm to the cortical label. **(b)** Whole trial HFA power time course. **(c)** Working memory period for HFA time course. **(d)** HFA decoding analyses for IFG contacts for all subjects **(e)** Time-domain decoding analysis from the iERP data. The decoding results have been thresholded based on a cluster-based maximum-statistic permutation test in each subject (p<0.05).

The HFA decoding results were plotted in a normalized Colin27-space as weighted averages of subject-contacts with significant decoding per label in a Laus500 parcellation atlas. The results over time during WM maintenance showed dynamic WM information representation throughout areas in the brain. Our widespread brain coverage (1180 cortical and subcortical contacts) findings demonstrated that content-specific information is transient within the brain regions as well as spread across the cortical hierarchy (Fig. 6-7).

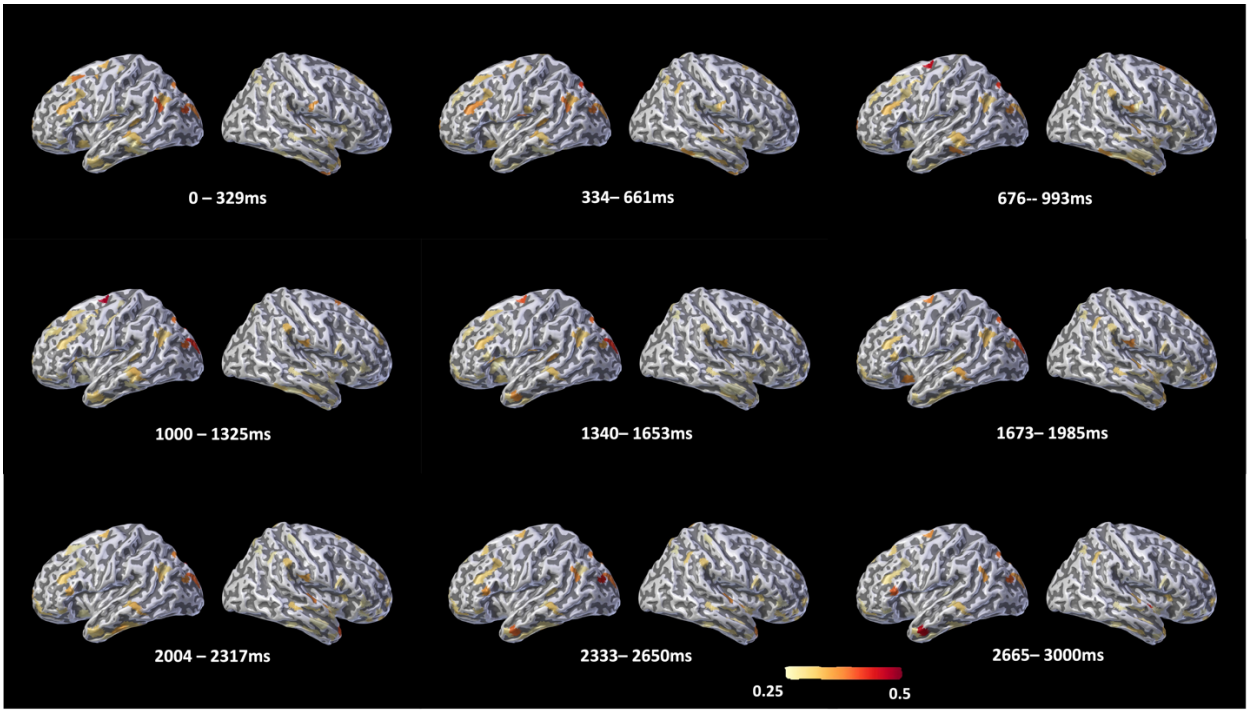

Figure 6. Time course of whole brain weighted decoding averaged in common space. The WM decoding accuracies were normalized to 9 frames from 180 time points. Weighted values were created as explained in *Methods subsection HFA Decoding Analysis.*

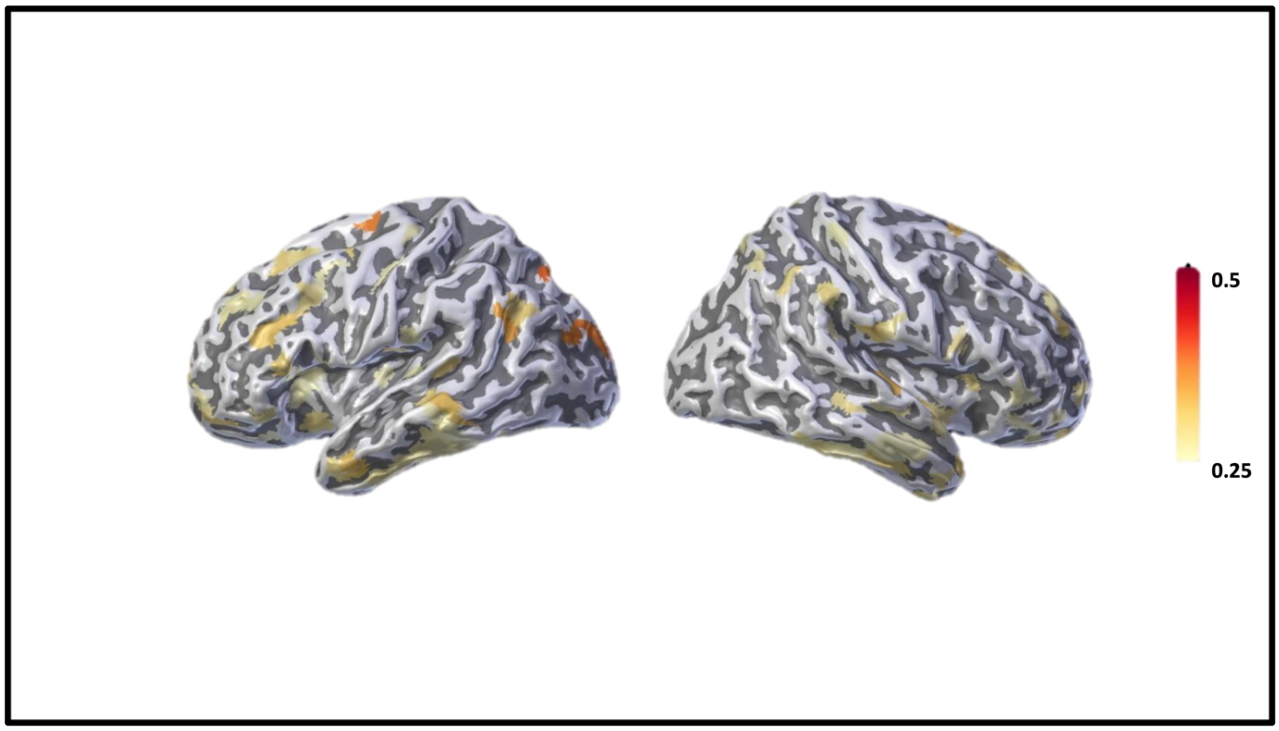

Figure 7. Whole brain weighted decoding averaged across whole WM period. The WM decoding accuracies were averaged across time and the weighted values were created as explained in *Methods subsection HFA Decoding Analysis.*

Multivariate Pattern Analysis of iERPs during WM Maintenance

To investigate WM information embedded in the temporal fine structure of dynamic sEEG activity, we conducted a time-domain iERP classification analysis. In our four-class SVM classification, we used the temporal information of trial-specific iERP signals within sliding 500-ms across the WM maintenance period. In the iERP decoding analysis, as in the HFA decoding, we found WM information decodable from different cortical or subcortical contacts in all subjects (Figures 2-5).

This temporal decoding analysis showed significant decoding clusters in all ten subjects that had sEEG contacts in ACs. Significant decoding results extended across the whole WM retention

period in six of these ten subjects (Fig. 2e). Overall, significant decoding results were observed in a larger number of contacts in iERP than HFA decoding in AC. However, in HFA analysis, there was more evidence of significant decoding in a single contact across the entire maintenance period.

In IFG, significant iERP decoding results were, again, found in all 11 subjects that had contacts in this area. In five of these subjects, decoding results significantly above chance level extended across the entire 3-s maintenance period. In another three subjects, significant results were very strongly present in either in the earlier or later delay period (Fig. 33). Similar to the contact channels in AC, IFG channels in HFA had longer periods of continuous significant decoding accuracy.

WM content could also be decoded from OFG in all ten subjects having contacts in this area. In five of these, significant decoding results emerged on and off throughout maintenance period (Fig. 4e). While the number of contacts showing significant results was larger than in iERP decoding, there was more evidence of significant results encompassing the entire maintenance period in one contact in HFA analysis in OFG.

Finally, our SVM analysis on HC contacts revealed significant decoding in contacts in eight out of ten subjects, 5 of which has contacts with over-chance decoding spread in the WM maintenance period (Fig. 5e). Comparison of these results to HFA decoding again presented contacts with longer significant accuracy periods in HFA classification.

Evolution of HFA Power across WM Encoding, Maintenance, and Recall Stages

To examine maintenance related activation patterns, we analyzed the evolution of 70-190 Hz HFA, a putative correlate of local firing activity, in epochs encompassing the entire trial period. In this analysis, the signal power was compared to the period preceding the presentation (and encoding) of the first item. We especially wanted to see if any continuous HFA would occur during periods where significant decoding could be shown. Our results show no evidence of significant

sustained elevation of HFA power in AC in contacts during maintenance period except for reaction to impulse sound stimuli, especially time-periods with significant WM decoding results, even in uncorrected t-tests across trials. In contrast to persistent increases, HFA effects show a significant decrease in power in most of the contacts (Fig. 2c). As for lateral PFC areas that have historically been linked to WM maintenance via persistent firing activity (REF), we found evidence of sparse HFA increases in IFG. However, the general maintenance period of most of the contacts again dominated by a reduction in power (Fig. 3c). OFG, contacts also show HFA power elevation sparsely during maintenance, but we mostly observe reduction in HFA during WM maintenance across different contacts (Fig. 4c). HC contacts show a pattern consistent with other areas, exhibiting a decrease in power throughout the WM maintenance period (Fig. 5c). For all the contacts that showed reduction in HFA power, none of them presented a similar pattern to the decoding accuracy patterns and were not always in channels with significant decoding accuracy.

Control Analyses

HFA Decoding of Uncued memory items

As a control, we have performed a four-class classification with an SVM classifier with the same parameters in the BHA decoding analysis on uncued stimuli. Our results have shown no significant decoding in any of the relevant contacts.

Discussion

The focus of investigation in the mechanisms of WM have recently shifted from where the information is stored to what are the nature of processes that enable WM maintenance (Lorenc and Sreenivasan, 2021). To this end, here, we employed intracranial SEEG depth electrode recordings to test whether the information is maintained by persistent activity or a more dynamic system of activities. We specifically examined whether WM representations are maintained via persistent elevation of neuronal activity or by a combination of more dynamic and activity-silent processes (Goldman-Rakic, 1995; Stokes, 2015) (for a discussion see, Lundqvist et al, 2018 and Constantinidis et al, 2018). In this context, we found evidence of content-specific WM representations carried by HFA, a putative correlate of multiunit firing activity, located in auditory, frontal areas and hippocampal regions. Our temporal pattern decoding results, which examined WM content in 500-ms windows of unfiltered iERP epochs, showed qualitatively similar decoding accuracy patterns from those areas. However, the HFA or temporal pattern decoding results, which were statistically significant according to our non-parametric permutation testing, were not accompanied with persistent increases of HFA power in comparison to the pre-trial baseline. Interestingly, in all areas of interest including higher order areas, HFA power significantly reduced in several contacts during WM maintenance, while the other contacts did not show any significant increase or decrease in HFA power. Most importantly, although some of the HFA power reduction could be denoted by the WM maintenance period, the spatiotemporal patterns of significant decoding and HFA power changes did not seem to overlap in any of our ROIs. These results are in line with an interpretation that WM maintenance is supported by a dynamic system of which processes does not depend on persistent increases of neuronal activity in a specific brain region.

HFA has been proposed as a reliable indicator of neuronal firing near deep electrodes (Ray et al., 2008; Ray and Maunsell, 2011; Leszczynski et al., 2020). Its correlate multiunit activity is proposed to be a component of WM in the PFC persistent albeit not stationary throughout the WM period (Fuster et al., 2000; Mendoza-Halliday et al., 2014; Vergara et al., 2016; Constantinidis et al., 2018). Constantinidis and colleagues (2018) discussed, in an illuminating debate with Lundqvist

et al, that the persistent activity in the lateral PFC enables the WM maintenance. Although the persistent firing code is not presumed to reflect stationary activity at the level of individual units, a proportion of neurons underlying WM maintenance should be active at least in a consistent pattern during the delay period. In other words, the premise is that maintenance-related persistent activity is based on population coding, which should also be reflected in persistently elevated patterns of HFA (Constantinidis et al., 2018). In contrast to this hypothesis, our results show little evidence of elevated HFA -stationary or non-stationary- in contacts showing evidence of content-specific HFA or iERP temporal patterns.

On the contrary, our decoding results suggest a more dynamic process, with a significant reduction in overall activity during maintenance, rather than a persistent activity (Mongillo et al., 2008; Barak et al., 2010; Barak and Tsodyks, 2014; Lundqvist et al., 2018a). Our decoding results show that content-specific information can be decoded from multiple brain regions including frontal and auditory regions as well as hippocampus. The information could be decoded in continuous chunks for a considerable part of the maintenance period. However, the WM decoding seems to alter through time in these contacts. These stable but not uniform decoding accuracies suggest a more dynamic WM maintenance rather than processes consistently contained in localized neuronal populations (Stokes, 2015).

Robust decoding of WM content was found not only in frontal contacts, but also in several of the contacts in or near AC. Consistent with the sensory recruitment model, we could decode in content specific WM information from contacts both in earlier areas (HG, superior temporal plane) and in higher areas of lateral STG and STG/superior temporal sulcus (STS) boundary(Uluç et al., 2018; Mamashli et al., 2021; Ahveninen et al., 2023). The sensory recruitment model of WM has been countered with evidence that information-containing activation patterns sensory areas such as AC are not as resistant to intervening distractors than in higher areas (Xu, 2017). Indeed, in certain contacts of AC, we did observe that decoding drops to chance level during the strong feedforward activation pattern to the unrelated distractor (or “impulse” sound) (Fig 2 C). However, in many of these contacts, the classifier performance rebounded after the strong feed-forward HFA to the impulse sound. Using the impulse sound, Wolff and colleagues (2017) address

the challenge of evidencing activity silent dynamic states as neuronal underpinnings of WM maintenance. With a disruption approach, they demonstrate that a response to an irrelevant impulse stimulus reflects memory specific information. Compatible with their findings, in our study, some of AC channels have shown significant decoding accuracy increase after impulse sound compatible with hidden state transitions that are coding WM information (Rose et al., 2016; Wolff et al., 2017).

The significance of HC in episodic memory is well established well established(Burgess et al., 2002; Moscovitch et al., 2016). In addition to this, a growing selection of studies show that HC has a critical role in working memory processing as well as episodic memory processes (Cabeza et al., 2002; Ezzyat and Olson, 2008; Axmacher et al., 2009; Leszczynski, 2011; Borders et al., 2022). However, HC's role in WM processing has been challenged by other studies (Baddeley et al., 2011) Compatible with research showing HC to be an integral part of WM, our results also show involvement of hippocampus in WM maintenance (Fig.XXC). Our decoding analysis showed that WM information could be found in the HFA from contacts recording from HC. Borders and colleagues (2021) suggest that HC plays the precise role of supporting complex high-precision binding in WM. Our study design does not allow us to investigate the precision of auditory WM but our results show that HC is involved in maintenance of complex sounds. In combination with the findings in other AC and frontal areas, our results point to a highly dynamic network distributed across several brain areas that is supported by activity silent processes as the neural correlate of WM maintenance.

Our results also suggest that some of the contacts from which we could decode WM content information show persistent suppression confined to the WM maintenance period. This is consistent with reports of several fMRI studies (Linke et al., 2011; Ahveninen et al., 2023; Deutsch et al., 2023), as well as with recent multi-site neurophysiological studies that reported suppressed firing in certain brain areas during maintenance (Dotson et al., 2018; Miller et al., 2018). Linke and colleagues have shown that instead of a robust content-specific activation, suppression in fMRI activity in sensory areas enable WM maintenance and dependent on the

rehearsal strategy of the participant (Linke et al., 2011). They argue that the suppression might be a natural gatekeeping mechanism against distractors.

In conclusion, our study shows that neuronal processes underlying WM maintenance are highly dynamic processes that are spread across sensory and frontal areas as well as HC. These results are in line with the hypothesis that WM maintenance can be supported by highly dynamic activity silent processes rather than persistent activity.

References

Ahveninen J, Uluc I, Raij T, Nummenmaa A, Mamashli F (2023) Spectrotemporal content of human auditory working memory represented in functional connectivity patterns. Commun Biol 6:294.

Axmacher N, Elger CE, Fell J (2009) Working memory-related hippocampal deactivation interferes with long-term memory formation. J Neurosci 29:1052-1960.

Baddeley A, Jarrold C, Vargha-Khadem F (2011) Working memory and the hippocampus. J Cogn Neurosci 23:3855-3861.

Baddeley AD, Hitch G (1974) Working Memory. Psychology of Learning and Motivation 8:47-89.

Barak O, Tsodyks M (2014) Working models of working memory. Curr Opin Neurobiol 25:20-24.

Barak O, Tsodyks M, Romo R (2010) Neuronal population coding of parametric working memory. J Neurosci 30:9424-9430.

Bastos AM, Loonis R, Kornblith S, Lundqvist M, Miller EK (2018) Laminar recordings in frontal cortex suggest distinct layers for maintenance and control of working memory. Proc Natl Acad Sci U S A 115:1117-1122.

Bigelow J, Poremba A (2014) Achilles' ear? Inferior human short-term and recognition memory in the auditory modality. PLoS One 9:e89914.

Borders AA, Ranganath C, Yonelinas AP (2022) The hippocampus supports high-precision binding in visual working memory. Hippocampus 32:217-230.

Burgess N, Maguire EA, O'Keefe J (2002) The human hippocampus and spatial and episodic memory. Neuron 35:625-641.

Cabeza R, Dolcos F, Graham R, Nyberg L (2002) Similarities and differences in the neural correlates of episodic memory retrieval and working memory. Neuroimage 16:317-330.

Chang C-C, Lin C-J (2011) LIBSVM: A library for support vector machines. ACM Trans Intell Syst Technol 2:1-27.

Christophel TB, Haynes JD (2014) Decoding complex flow-field patterns in visual working memory. NeuroImage 91:43-51.

Christophel TB, Hebart MN, Haynes J-D (2012) Decoding the contents of visual short-term memory from human visual and parietal cortex. The Journal of neuroscience : the official journal of the Society for Neuroscience 32:12983-12989.

Christophel TB et al. (2017) The Distributed Nature of Working Memory. Trends in Cognitive Sciences 0:115-142.

Constantinidis C, Procyk E (2004) The primate working memory networks. Cogn Affect Behav Neurosci 4:444-465.

Constantinidis C, Funahashi S, Lee D, Murray JD, Qi XL, Wang M, Arnsten AFT (2018) Persistent Spiking Activity Underlies Working Memory. J Neurosci 38:7020-7028.

D'Esposito M, Postle BR (2015) The Cognitive Neuroscience of Working Memory. Annual Review of Psychology 66:115-142.

Daducci A, Gerhard S, Griffa A, Lemkaddem A, Cammoun L, Gigandet X, Meuli R, Hagmann P, Thiran JP (2012) The connectome mapper: an open-source processing pipeline to map connectomes with MRI. PLoS One 7:e48121.

Desikan RS, Segonne F, Fischl B, Quinn BT, Dickerson BC, Blacker D, Buckner RL, Dale AM, Maguire RP, Hyman BT, Albert MS, Killiany RJ (2006) An automated labeling system for subdividing the human cerebral cortex on MRI scans into gyral based regions of interest. Neuroimage 31:968-980.

Deutsch P, Czoschke S, Fischer C, Kaiser J, Bledowski C (2023) Decoding of Working Memory Contents in Auditory Cortex Is Not Distractor-Resistant. J Neurosci 43:3284-3293.

Dotson NM, Hoffman SJ, Goodell B, Gray CM (2018) Feature-Based Visual Short-Term Memory Is Widely Distributed and Hierarchically Organized. Neuron 99:215-226 e214.

Ezzyat Y, Olson IR (2008) The medial temporal lobe and visual working memory: comparisons across tasks, delays, and visual similarity. Cogn Affect Behav Neurosci 8:32-40.

Fischl B, van der Kouwe A, Destrieux C, Halgren E, Segonne F, Salat DH, Busa E, Seidman LJ, Goldstein J, Kennedy D, Caviness V, Makris N, Rosen B, Dale AM (2004) Automatically parcellating the human cerebral cortex. Cereb Cortex 14:11-22.

Fritz J, Mishkin M, Saunders RC (2005) In search of an auditory engram. Proc Natl Acad Sci U S A 102:9359-9364.

Fuster JM, Alexander GE (1971) Excitation and Inhibition of Neuronal Firing in Visual Cortex by Reticular Stimulation. Science 133:2011-2012.

Fuster JM, Bodner M, Kroger JK (2000) Cross-modal and cross-temporal association in neurons of frontal cortex. Nature 405:347-351.

Goldman-Rakic PS (1995) Cellular basis of working memory. Neuron 14:477-485.

Gottlieb Y, Vaadia E, Abeles M (1989) Single unit activity in the auditory cortex of a monkey performing a short term memory task. Exp Brain Res 74:139-148.

Howard MW, Rizzuto DS, Caplan JB, Madsen JR, Lisman J, Aschenbrenner-Scheibe R, Schulze-Bonhage A, Kahana MJ (2003) Gamma oscillations correlate with working memory load in humans. Cereb Cortex 13:1369-1374.

Kaiser J (2015) Dynamics of auditory working memory. Front Psychol 6:613.

Kaiser J, Heidegger T, Wibral M, Altmann CF, Lutzenberger W (2007) Alpha synchronization during auditory spatial short-term memory. Neuroreport 18:1129-1132.

Kaiser J, Heidegger T, Wibral M, Altmann CF, Lutzenberger W (2008) Distinct gamma-band components reflect the short-term memory maintenance of different sound lateralization angles. Cereb Cortex 18:2286-2295.

Kucewicz MT, Berry BM, Kremen V, Brinkmann BH, Sperling MR, Jobst BC, Gross RE, Lega B, Sheth SA, Stein JM, Das SR, Gorniak R, Stead SM, Rizzuto DS, Kahana MJ, Worrell GA (2017) Dissecting gamma frequency activity during human memory processing. Brain 140:1337-1350.

Kumar S, Joseph S, Gander PE, Barascud N, Halpern AR, Griffiths TD (2016) A Brain System for Auditory Working Memory. The Journal of neuroscience : the official journal of the Society for Neuroscience 36:4492-4505.

Leszczynski M (2011) How does hippocampus contribute to working memory processing? Front Hum Neurosci 5:168.

Leszczynski M, Barczak A, Kajikawa Y, Ulbert I, Falchier AY, Tal I, Haegens S, Melloni L, Knight RT, Schroeder CE (2020) Dissociation of broadband high-frequency activity and neuronal firing in the neocortex. Sci Adv 6:eabb0977.

Linke AC, Vicente-Grabovetsky A, Cusack R (2011) Stimulus-specific suppression preserves information in auditory short-term memory. Proceedings of the National Academy of Sciences of the United States of America 108:12961-12966.
Lundqvist M, Herman P, Miller EK (2018a) Working Memory: Delay Activity, Yes! Persistent Activity? Maybe Not. J Neurosci 38:7013-7019.
Lundqvist M, Herman P, Warden MR, Brincat SL, Miller EK (2018b) Gamma and beta bursts during working memory readout suggest roles in its volitional control. Nat Commun 9:394.
Lundqvist M, Rose J, Herman P, Brincat SL, Buschman TJ, Miller EK (2016) Gamma and Beta Bursts Underlie Working Memory. Neuron 90:152-164.
Lutzenberger W, Ripper B, Busse L, Birbaumer N, Kaiser J (2002) Dynamics of gamma-band activity during an audiospatial working memory task in humans. J Neurosci 22:5630-5638.
Mamashli F, Khan S, Hamalainen M, Jas M, Raij T, Stufflebeam SM, Nummenmaa A, Ahveninen J (2021) Synchronization patterns reveal neuronal coding of working memory content. Cell Rep 36:109566.
Medalla M, Barbas H (2014) Specialized prefrontal "auditory fields": organization of primate prefrontal-temporal pathways. Front Neurosci 8:77.
Mendoza-Halliday D, Torres S, Martinez-Trujillo JC (2014) Sharp emergence of feature-selective sustained activity along the dorsal visual pathway. Nature Neuroscience 17:1255-1262.
Miller EK, Lundqvist M, Bastos AM (2018) Working Memory 2.0. Neuron 100:463-475.
Mongillo G, Barak O, Tsodyks M (2008) Synaptic theory of working memory. Science 319:1543-1546.
Moscovitch M, Cabeza R, Winocur G, Nadel L (2016) Episodic Memory and Beyond: The Hippocampus and Neocortex in Transformation. Annu Rev Psychol 67:105-134.
Ng CW, Plakke B, Poremba A (2014) Neural correlates of auditory recognition memory in the primate dorsal temporal pole. J Neurophysiol 111:455-469.
Oostenveld R, Fries P, Maris E, Schoffelen JM (2011) FieldTrip: Open source software for advanced analysis of MEG, EEG, and invasive electrophysiological data. Comput Intell Neurosci 2011:156869.
Oosterhof NN, Connolly AC, Haxby JV (2016) CoSMoMVPA: Multi-Modal Multivariate Pattern Analysis of Neuroimaging Data in Matlab/GNU Octave. Front Neuroinform 10:27.
Ray S, Maunsell JH (2011) Different origins of gamma rhythm and high-gamma activity in macaque visual cortex. PLoS Biol 9:e1000610.
Ray S, Crone NE, Niebur E, Franaszczuk PJ, Hsiao SS (2008) Neural correlates of high-gamma oscillations (60-200 Hz) in macaque local field potentials and their potential implications in electrocorticography. J Neurosci 28:11526-11536.
Reuter M, Rosas HD, Fischl B (2010) Highly accurate inverse consistent registration: a robust approach. Neuroimage 53:1181-1196.
Reuter M, Schmansky NJ, Rosas HD, Fischl B (2012) Within-subject template estimation for unbiased longitudinal image analysis. Neuroimage 61:1402-1418.
Romo R, Brody CD, Hernández A, Lemus L (1999) Neuronal correlates of parametric working memory in the prefrontal cortex. Nature 399:470-473.

Rose NS, LaRocque JJ, Riggall AC, Gosseries O, Starrett MJ, Meyering EE, Postle BR (2016) Reactivation of latent working memories with transcranial magnetic stimulation. Science 354:1136-1139.
Rosenkilde CE, Bauer RH, Fuster JM (1981) Single cell activity in ventral prefrontal cortex of behaving monkeys. Brain Res 209:375-394.
Sakurai Y (1990) Hippocampal cells have behavioral correlates during the performance of an auditory working memory task in the rat. Behav Neurosci 104:253-263.
Schmidt TT, Wu Y-h, Blankenburg F (2015) Print |Close PFC maintains abstract quantitative but not spatial tactile stimulus features during working memory. In: OHBM 2015.
Scott BH, Mishkin M (2016) Auditory short-term memory in the primate auditory cortex. Brain Res 1640:264-277.
Scott BH, Mishkin M, Yin P (2012) Monkeys have a limited form of short-term memory in audition. Proc Natl Acad Sci U S A 109:12237-12241.
Scott BH, Mishkin M, Yin P (2014) Neural correlates of auditory short-term memory in rostral superior temporal cortex. Curr Biol 24:2767-2775.
Shafi M, Zhou Y, Quintana J, Chow C, Fuster J, Bodner M (2007) Variability in neuronal activity in primate cortex during working memory tasks. Neuroscience 146:1082-1108.
Shamma S (2001) On the role of space and time in auditory processing. Trends Cogn Sci 5:340-348.
Soper DJ, Reich D, Ross A, Salami P, Cash SS, Basu I, Peled N, Paulk AC (2023) Modular pipeline for reconstruction and localization of implanted intracranial ECoG and sEEG electrodes. PLoS One 18:e0287921.
Sreenivasan KK, D'Esposito M (2019) The what, where and how of delay activity. Nat Rev Neurosci 20:466-481.
Stokes MG (2015) 'Activity-silent' working memory in prefrontal cortex: a dynamic coding framework. Trends Cogn Sci 19:394-405.
Uluç I, Schmidt TT, Wu YH, Blankenburg F (2018) Content-specific codes of parametric auditory working memory in humans. NeuroImage 183.
Vergara J, Rivera N, Rossi-Pool R, Romo R (2016) A Neural Parametric Code for Storing Information of More than One Sensory Modality in Working Memory. Neuron 89:54-62.
Wolff MJ, Jochim J, Akyurek EG, Stokes MG (2017) Dynamic hidden states underlying working-memory-guided behavior. Nat Neurosci 20:864-871.
Wu Y-h, Uluç I, Schmidt TT, Tertel K, Kirilina E, Blankenburg F (2018) Overlapping frontoparietal networks for tactile and visual parametric working memory representations. NeuroImage 166:325-334.
Xu Y (2017) Reevaluating the Sensory Account of Visual Working Memory Storage. Trends Cogn Sci 21:794-815.
Yamamoto J, Suh J, Takeuchi D, Tonegawa S (2014) Successful execution of working memory linked to synchronized high-frequency gamma oscillations. Cell 157:845-857.